Energy 253 (2022) 124126

Contents lists available at ScienceDirect

Energy

journal homepage: www.elsevier.com/locate/energy

Comparative study on cooling method for concentrating photovoltaic system

Yishuang Ji [a], Song Lv [a, b, *], Zuoqin Qian [a], Yitong Ji [b], Juwen Ren [a], Kaiming Liang [a], Shulong Wang [a]

[a] Key Laboratory of High Performance Ship Technology, Ministry of Education, School of Naval Architecture, Ocean and Energy Power Engineering, Wuhan University of Technology, Wuhan, 430063, China
[b] School of Materials Science and Engineering, Wuhan University of Technology, Wuhan, 430063, China

ARTICLE INFO

Article history:
Received 7 November 2021
Received in revised form
24 April 2022
Accepted 25 April 2022
Available online 1 May 2022

Keywords:
Concentrating photovoltaic
Heat exchanger
Numerical analysis
Pump consumption
Electrical exergy efficiency

ABSTRACT

Concentrating photovoltaic technology has been one of the important technologies among renewable energy technologies. Researchers have used one or more cooling methods to increase the output power by cooling the CPV cells. In this work, CPV systems with three typical cooling methods of air cooling, water cooling and heat pipe cooling have been comparatively studied. An Outdoor experiment was conducted under the same environmental conditions. The pump power loss factor was considered to evaluate the thermal and electrical performance of the three systems. The experimental results indicate that the average temperatures of the finned heatsink, water cooling module, and heat pipe during the test are 41 °C, 25.9 °C and 22.2 °C, respectively. The CPV cell with heat pipe cooling method exhibits the highest output power of 8.27 W. When the pump consumption is considered, the water-cooled CPV cell can provide the highest net electrical efficiency of 28.3% and electrical exergy efficiency of 30.4%. In addition, a thermal-electrical coupling model was established to investigate the effects of different parameters, such as inlet fluid temperature, mass flow rate and concentration ratio on CPV system. The results can provide some practical guidelines for the design and application of practical CPV cooling systems.

1. Introduction

People have paid more attention to exploit and utilize renewable energy due to the growth demand of energy and the shortage of fossil fuels. As a green energy with abundant reserves, wide distribution, clean and free, solar energy has attracted extensive attention to meet the challenges [1]. At present, among many solar energy utilization technologies, the most widely used technology is photovoltaic technology. In order to solve the problem of low solar energy density and improve the photoelectric conversion efficiency of photovoltaic (PV) cells, the concentrating structure is generally used. The incident sunlight is concentrated on the surface of the cell to increase the density of convertible photons, which can excite electron and hole pairs in the active layer of the cell [2]. However, due to the restriction of the conversion efficiency of PV cells, the photons absorbed by the cell cannot be completely converted and utilized. Some photons will be converted into waste heat, which will cause the temperature of the PV cell to rise. After using the concentrating structure, the problem of higher focal temperature of the PV cell is more critical, which is harmful to its conversion efficiency and reliability [3–6]. In order to avoid the excessive temperature of the PV cell, a cooling system was usually used to eliminate the adverse effects of the increasing PV temperature. Researchers have used one or more of the cooling methods to increase the output power by cooling the CPV cells. These cooling systems can be classified as air flow [7–10], liquid cooling [11–15], heat pipe [16–21], thermoelectric [22–24], phase change material [25–27], liquid immersion [28,29], coating by spectral splitting filter [30–32], microchannel [33,34]. Each cooling technique has positive effects on the CPV system in the literature. Compared with other cooling technologies, the three most commonly used cooling technologies, air flow, liquid cooling and heat pipe, have relatively low initial cost, simple structure, and their cooling effect can reach

* Corresponding author. Key Laboratory of High Performance Ship Technology, Ministry of Education, School of Naval Architecture, Ocean and Energy Power Engineering, Wuhan University of Technology, Wuhan, 430063, China.
E-mail address: lvsong@whut.edu.cn (S. Lv).

https://doi.org/10.1016/j.energy.2022.124126
0360-5442/

an acceptable level [2].

Aldossary et al. [35] examined the surface temperature and electrical performance of a CPV cell using round pin heatsink, straight fins heatsink and water channel under high solar concentration in where ambient temperature can reach up to 50 °C. Al-Amri and Mallick [8] predicted the maximum temperature of solar cell cooled actively by air-mixed convection with and without the interaction of radiation. It was found that the maximum cell temperature and the critical concentration ratio are extremely dependent on air inlet velocity, channel width, thicknesses and thermal conductivities of the holders and accessories. Chen et al. [36] investigated the performance of a high CPV system which incorporates lens and water-cooling tube, and they found that the instantaneous electrical efficiency and thermal efficiency of the HCPV system were respectively 26.5% and 49.3%, the average thermal efficiency was 46.8%. Anderson et al. [37] discussed a cooling design that used a copper/water heat pipe with aluminum fins to cool a CPV cell by natural convection. According to their report, when the input heat flux is 40 W/cm^2, the temperature difference between the cell using the heat pipe and the environment is only 40 °C. Farahat et al. [38] comparatively investigated the effect of the actual temperature on the performance of a PV cell by using heat pipe cooling and water cooling technique. Lee and Baek [39] proposed a CPV system using a thermal absorber containing heat pipes and cooling water. It has been reported that the average electrical and thermal efficiency were 20% and 77%, respectively.

Based on above literature survey, few literatures focus on the impact of the power consumption of auxiliary equipment used for cooling such as pump or fan, on the CPV system. A comparative study is not available for the comparison of thermal and electrical performance enhancement of CPV system by using the three most commonly used active cooling methods of airflow, liquid and heat pipe under the same environmental and operating conditions. In this context, the novelty of our work is that a comparative study is performed on CPV systems using three typical cooling methods (air cooling, water cooling, heat pipe cooling), and the effect of pump power loss on CPV system performance is considered. The corresponding analytical all-parameter models of thermal-electrical coupling are proposed, and the accuracy of the models is verified by continuous outdoor test. It indicates that the models can be further generalized to the analysis and optimization of PV farms. Furthermore, the effects of different parameters, such as inlet fluid temperature, mass flow rate and concentration ratio on output power, electrical efficiency and electrical exergy efficiency of CPV cells were analyzed. The contribution of this work is that the results can provide some practical guidelines for the design and application of practical CPV cooling systems.

2. Models

2.1. Thermal model of CPV system

CPV system is composed by a set of solar collecting components and photoelectric conversion devices. Fig. 1 shows a schematic of a typical CPV system consisting of a Fresnel lens, an optical prism, a PV cell and a thermal conductive plate. Solar radiation is concentrated to the surface of the PV cell through the Fresnel lens and optical prism. The heat transfer between the absorber plate with high thermal conductivity and the PV cell is through thermal contact with silicone grease. Different cooling modules are placed on the bottom of the absorber plate to improve the photoelectric conversion efficiency.

The heat transfer model of the typical CPV system can be discussed by the heat transfer network illustrated in Fig. 2. The dynamic

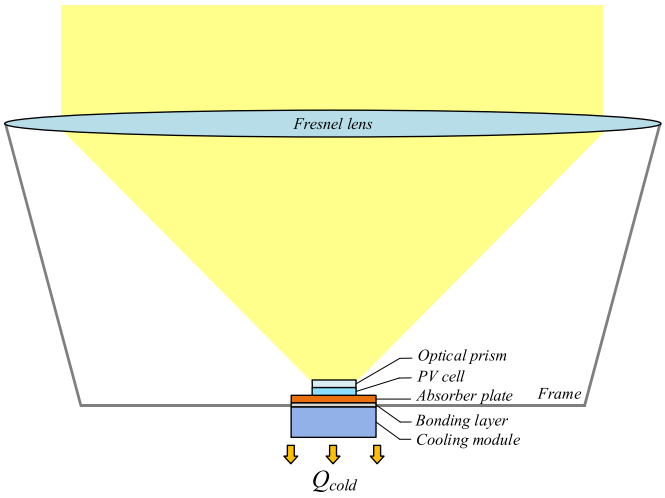

Fig. 1. Schematic diagram of CPV system.

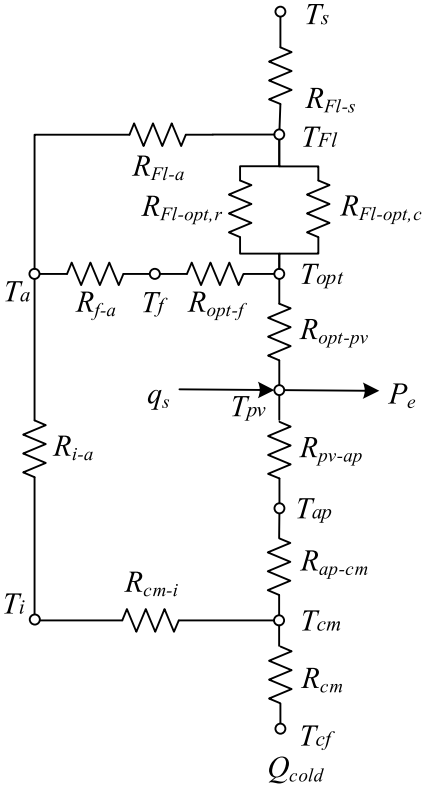

Fig. 2. Schematic of the heat transfer network of CPV system.

energy balance for each part of the system can be defined after making the following assumptions: (a) heat transfer is one-dimensional, each component has its own temperature and capacitance, which can be considered as the average temperature of its surface; (b) The Fresnel lens and optical prism are ideal and clean with the negligible effect of dust and dirty, and the optical energy loss of Fresnel lens and optical prism is uniformly expressed by optical efficiency; (c) The solar energy concentrated on the surface of the PV cell through the Fresnel lens and optical prism is considered to be uniform due to its very small area; (d) The properties of all materials are constant, while all thermophysical properties of cooling medium have been considered temperature dependent.

- For the Fresnel lens

Fresnel lens is an optical system and mainly solar radiation is transmitted and finally absorbed by the optical prism and PV cell. The Fresnel lens exchanges heat via convection heat transfer with the ambient air and the optical prism, radiation heat transfer with the sky and the optical prism. The heat transfer mechanism acts could be given by,

$$\alpha_{Fl} C A_{pv} I_s = \frac{T_{Fl} - T_s}{R_{Fl-s}} + \frac{T_{Fl} - T_a}{R_{Fl-a}} + \frac{T_{Fl} - T_{opt}}{R_{Fl-opt,c}} + \frac{T_{Fl} - T_{opt}}{R_{Fl-opt,r}} \tag{1}$$

where α_{Fl} is the absorptance of Fresnel lens, C is the concentration ratio of system, A_{PV} is the area of PV cell; I_s is the solar irradiance; T_{Fl} is the temperature of Fresnel lens; T_s is the temperature of sky, $T_s = 0.0552 \cdot {T_a}^{1.5}$; T_a is the temperature of ambient air; T_{opt} is the temperature of optical prism; R_{Fl-s} and R_{Fl-a} are the thermal resistance of the radiation heat transfer between Fresnel lens and sky and the convection heat transfer between Fresnel lens and ambient air; $R_{Fl-opt,c}$ and $R_{Fl-opt,r}$ are the thermal resistance of convection and radiation heat transfer between Fresnel lens and optical prism. Overall thermal resistance can be obtained from Refs. [36,40,41],

$$R_{Fl-s} = \frac{1}{\varepsilon_{Fl}\sigma\left(T_{Fl}^2 + T_s^2\right)(T_{Fl} + T_s)A_{Fl}} \tag{2}$$

$$R_{Fl-a} = \frac{1}{(2.8 + 3u)A_{Fl}} \tag{3}$$

$$R_{Fl-opt,r} = \frac{1}{\varepsilon_{opt}\sigma\left(T_{opt}^2 + T_{FL}^2\right)(T_{opt} + T_{Fl})A_{opt}F_{opt-Fl}} \tag{4}$$

$$R_{Fl-opt,c} = \frac{1}{A_{Fl}h_{air}} \tag{5}$$

$$h_a = \frac{Nu \cdot K_{air}}{H} \tag{6}$$

$$Nu = 0.7681 \cdot \left(0.25^{0.25} + 0.75^{0.25}\right) + 0.0248 \cdot Ra^{0.4345} \tag{7}$$

In the above equations, ε_{Fl} and ε_{opt} are the emissivity of Fresnel lens and optical prism, respectively; σ is Boltzmann constant; u is the velocity of wind; A_{opt} and A_{Fl} are the area of optical prism and Fresnel lens; F_{Fl-opt} is the coefficient of angularity between optical prism and Fresnel lens; h_a is the natural convection heat transfer coefficient of the internal air caused by the temperature difference between the optical prism and the Fresnel lens in the closed frame; K_{air} is the thermal conductivity of air; H is the distance between the optical prism and the Fresnel lens; Nu is the Nusselt number; and Ra is the Rayleigh number [41].

- For the optical prism

The incident solar energy is uniformly concentrated on the surface of the solar cell through the secondary optical prism. The energy balance equation could be calculated by Ref. [36]:

$$\tau_{Fl}\alpha_{opt}A_{Fl}I_s = \frac{T_{opt} - T_{Fl}}{R_{opt-Fl,r}} + \frac{T_{opt} - T_{Fl}}{R_{opt-Fl,c}} + \frac{T_{opt} - T_{pv}}{R_{opt-pv}} + \frac{T_{opt} - T_f}{R_{opt-f}} \tag{8}$$

where τ_{Fl} is the transmittance of Fresnel lens; α_{opt} is the absorptance of optical prism; T_{pv} and T_f are the temperature of PV cell and frame; R_{opt-f} is the thermal resistance between optical prism and frame; R_{opt-pv} is the thermal resistance between optical prism and PV cell. The thermal resistance could be expressed as follows:

$$R_{opt-pv} = \frac{\delta_{opt}}{k_{opt}A_{opt}} \tag{9}$$

$$R_{opt-f} = \frac{1}{\varepsilon_{opt}\sigma\left(T_{opt}^2 + T_f^2\right)\left(T_{opt} + T_f\right)A_{opt}F_{opt-f}} \tag{10}$$

where δ_{opt} and k_{opt} are the thickness and thermal conductivity of optical prism. F_{opt-f} is the coefficient of angularity between optical prism and frame.

- For the PV cell

The PV cell absorbs solar radiation concentrated by the Fresnel lens and exchanges heat through conduction heat transfer with absorber plate. The expression of the heat transfer mechanism could be given by Ref. [40]:

$$\tau_{opt}\tau_{Fl}\alpha_{PV}CA_{PV}I_s = E_p + \frac{T_{PV} - T_{opt}}{R_{PV-opt}} + \frac{T_{PV} - T_{ap}}{R_{PV-ap}} \tag{11}$$

where τ_{opt} is the transmittance of option prism; α_{pv} is the absorptance of PV cell; T_{ap} is the temperature of absorber plate; R_{pv-ap} is the thermal resistance between PV cell and absorber plate. The thermal resistance could be expressed as:

$$R_{PV-ap} = R_{PV} + R_{ce1} \tag{12}$$

where R_{pv} is the equivalent thermal resistance of PV cell; R_{ce1} is the thermal resistance of heat diffusion from PV cell to absorber plate.

- For the frame

The frame exchanges heat via convection heat transfer with ambient air and radiation heat transfer with PV cell. The energy balance equation could be given by,

$$\frac{T_{opt} - T_f}{R_{opt-f}} = \frac{T_f - T_a}{R_{f-a}} \tag{13}$$

$$R_{f-a} = \frac{1}{(2.8 + 3u)A_f} \tag{14}$$

where A_f is the area of frame; R_{f-a} is the thermal resistance of convection heat transfer between frame and ambient air.

- For the absorber plate

The absorber plate exchanges heat by conduction heat transfer to different cooling module. The expression of the energy balance equation could be given by,

$$\frac{T_{PV} - T_{ap}}{R_{PV-ap}} = \frac{T_{ap} - T_{cm}}{R_{ap-cm}} \tag{15}$$

$$R_{ap-cm} = \frac{\delta_{ap}}{k_{ap}A_{ap}} + R_{ce2} + \frac{\delta_{bl}}{k_{bl}A_{bl}} \tag{16}$$

where T_{cm} is the temperature of different cooling module; R_{ap-cm} is the thermal resistance between absorber plate and cooling module; R_{ce2} is the thermal resistance of heat diffusion from absorber plate to cooling module; δ_{ap}, k_{ap} and A_{ap} are the thickness, thermal conductivity and area of absorber plate. δ_{bl}, k_{bl} and A_{bl} are the thickness, thermal conductivity, and area of bonding layer.

- For the insulation

The insulation is used to isolate the heat transfer between the cooling module and the external environment to improve the cooling effect of different modules. Since the active air-cooling module is in direct contact with the external environment, the insulation is not considered in this module. The energy relationship can be expressed as:

$$\frac{T_{cm}-T_i}{R_{cm-i}}=\frac{T_i-T_a}{R_{i-a}} \tag{17}$$

$$R_{cm-i}=\frac{\delta_i}{k_i A_i} \tag{18}$$

$$R_{i-a}=\frac{1}{(2.8+3u)A_i} \tag{19}$$

where R_{cm-i} is the thermal resistance between cooling module and insulation; T_i, δ_i, k_i and A_i are the temperature, thickness, and area of insulation; R_{i-a} is the thermal resistance of the convection heat transfer between insulation and ambient air.

2.2. The analytic models of cooling methods

- For the air-cooling module

The first active cooling method is a cooling module with an air cooling exchanger, illustrated schematically in Fig. 3, consisting of a plate finned heatsink and a low-power fan.

$$\frac{T_{ap}-T_{cm1}}{R_{ap-cm}}=\frac{T_{cm1}-T_a}{R_{cm1}} \tag{20}$$

where R_{cm1} is thermal resistance of heat transfer by convection from boundaries to ambient air. According to literature [42], the formulas of calculating R_{cm1} are as follows:

$$R_{cm1}=\frac{1}{\eta_{fin}h_{air}A_{cm1}} \tag{21}$$

$$\eta_{fin}=\frac{th\left[\sqrt{\frac{h_{air}(2L_{cm1}+2\delta_{fin})}{k_{air}L_{cm1}\delta_{fin}}}\left(L_{cm1}+\frac{1}{2}\delta_{fin}\right)\right]}{\sqrt{\frac{h_{air}(2L_{cm1}+2\delta_{fin})}{k_{air}L_{cm1}\delta_{fin}}}\left(L_{cm1}+\frac{1}{2}\delta_{fin}\right)} \tag{22}$$

$$h_{air}=\frac{k_{air}Nu}{L_{cm1}} \tag{23}$$

$$Nu=\begin{cases}0.664Re^{\frac{1}{2}}Pr^{\frac{1}{3}}, Re\le 2300\\ 0.0296Re^{\frac{4}{5}}Pr^{\frac{1}{3}}, Re\ge 2300\end{cases} \tag{24}$$

where K_{air} is the thermal conductivity of and air; η_{fin} is the efficiency of fins, h_{fin} is the convection heat transfer coefficient of the heatsink; A_{cm1} is the contact area between air and heatsink; L_{cm1} is the length of heatsink; δ_{fin} is the thickness of fin; $Re=u_{air}L_{cm1}/\nu_{air}$ is the Reynolds number, $Pr=\nu_{air}/\alpha_{air}$ is the Prandtl number of air.

- For the water-cooling module

The second active cooling method is a cooling module with a water channel heat exchanger, illustrated schematically in Fig. 4, consisting of a water cooling heatsink, thermal insulation and cooling water.

$$\frac{T_{cm2}-T_w}{R_{cm2}}=m_w C_w(T_{out}-T_{in}) \tag{25}$$

where T_{cf2} is the temperature of cooling water; T_{out} and T_{in} are the outlet and inlet temperature of tube; $m_w=\rho_w\mu_w {D_h}^2$ is the mass velocity of water; C_w is the heat capacity of water; R_{cm2} is the thermal resistance of water-cooling module. According to literature [36,43], the formulas of calculating R_{cm2} are as follows:

$$R_{cm2}=\frac{1}{h_w A_{cm2}} \tag{26}$$

$$h_w=\frac{k_w Nu_w}{D_h} \tag{27}$$

$$Nu=\begin{cases}4.364, \mathrm{Re}<2300\\ 0.023Re^{0.8}Pr^{0.4}, Re>2300\end{cases} \tag{28}$$

where K_w is the thermal conductivity of water; h_w is the convection heat transfer coefficient between tube and water; A_{cm2} is the total

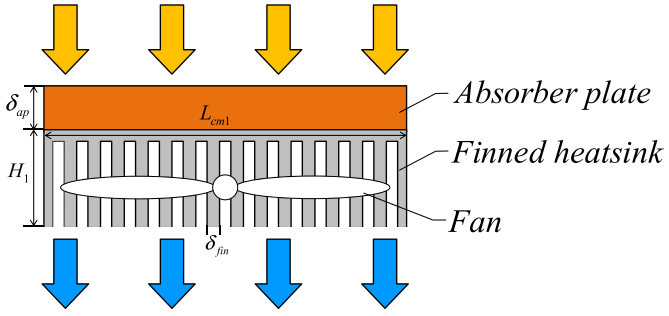

Fig. 3. The schematic diagram of CPV system with air-cooling module.

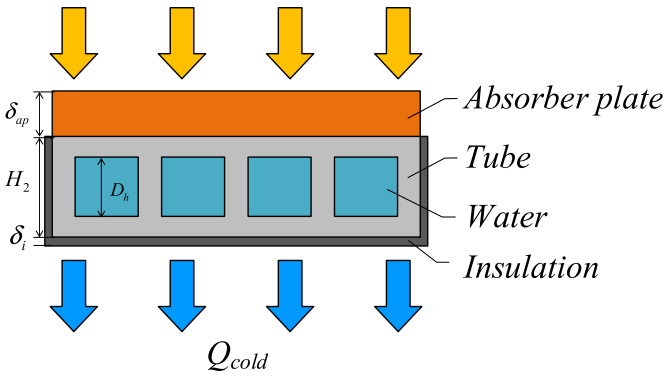

Fig. 4. The schematic diagram of CPV system with water-cooling module.

area of channels; D_h is the hydraulic diameter of channel; $Re = u_w D_h/\mu_w$ is the Reynolds number, $Pr = \mu_w/\alpha_w$ is the Prandtl number of the water.

- For the heat pipe module

The third active cooling method is a cooling module with a heat pipe exchanger, illustrated schematically in Fig. 5, consisting of a heat pipe, a tube, thermal insulation and cooling water.

$$\frac{T_{ap} - T_{cm3}}{R_{ap-cm}} = \frac{T_{cm3} - T_i}{R_{cm-i}} + \frac{T_{cm3} - T_w}{R_{cm3}} \tag{29}$$

According to literature [44,45], thermal resistance of cooling module 3 R_{cm3} could be given by,

$$R_{cm3} = R_{conf} + R_{ep} + R_{ec} + R_{cc} + R_{cp} + R_{covf} \tag{30}$$

where R_{conf} is the thermal resistance of heat transfer from the surface of absorber plate to the surface of the evaporation section of heat pipe; R_{ep} and R_{ec} are the equivalent thermal resistance of the pipe wall and capillary core in the evaporation section of heat pipe; R_{cc} and R_{cp} are the thermal resistance of the core and wall in the condensation section; R_{covf} is the thermal resistance of heat transfer by convection from condensation section of heat pipe to water. Overall thermal resistance of the heat sink can be obtained from Ref. [46],

$$R_{conf3} = R_{ct1} + \frac{H_{cm3}}{K_{cm3} S_{cm3}} \tag{31}$$

$$R_{ep} = \frac{ln(D_{op}/D_{ip})}{2\pi L_{ep} K_p} \tag{32}$$

$$R_{ec} = \frac{ln(D_{oc}/D_{ic})}{2\pi L_{ep} K_c} \tag{33}$$

$$R_{cc} = \frac{1}{\pi L_{ep} h_c} \tag{34}$$

$$R_{cp} = \frac{ln(D_{op}/D_{ip})}{2\pi L_{cp} K_p} \tag{35}$$

$$R_{covf3} = R_{ct2} + \frac{1}{h_w A_{cm3}} \tag{36}$$

$$h_w = \frac{Nu_w K_w}{D_{op}} \tag{37}$$

where R_{ct1} is the contact thermal resistance between absorber plate and heat pipe fixture; R_{ct2} is the contact thermal resistance between the condensing section of heat pipe and tube; H_{cm3}, K_{cm3} and S_{cm3} are the height, thermal conductivity and cross-sectional area of heat pipe fixture; D_{op} and D_{ip} are the outer and inner diameter of pipe; D_{oc} and D_{ic} are the outer and inner diameters of core; L_{ep} and L_{cp} are the length of the evaporation section and condensation section of heat pipe; K_p and K_c are the thermal conductivity of pipe and core; h_c is the condensation heat transfer coefficient between the working fluid and the inner wall of pipe; A_{cm3} is the contact area between cooling water and outer wall of heat pipe. The cooling water flows across the surface of the condensing section of heat pipe, which is the forced convection heat transfer of liquid across the tube. Nusselt number [46] is determined by,

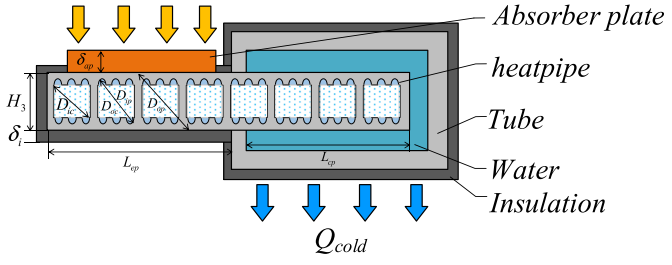

Fig. 5. The schematic diagram of CPV system with heat pipe module.

$$Nu = c \cdot Re^a \cdot Pr^b \cdot \left(\frac{Pr_\infty}{Pr_s}\right)^{\frac{1}{4}} \tag{38}$$

where the values of c, a and b depend on the Reynolds number and Prandtl number.

The main parameters needed for simulation are shown in the following Table 1.

2.3. Electrical model

The electrical output E_p in the thermal model is affected by the parameters of the PV cell, and is also restricted by the intensity of the radiation and the temperature of the PV cell. To simplify the model, the commonly used single diode model is adopted in this work. The multi-junction cell is regarded as a model with only a unified output voltage, current, series resistance and parallel resistance, which defined [47] as shown in Eq. (39):

$$I = L_L - I_o \left\{ \exp\left[\frac{q(V + IR_s)}{AkT}\right] - 1 \right\} - \frac{V + IR_s}{R_{sh}} \tag{39}$$

where I, V and T are the output current, voltage at load and temperature of PV cell; q is the charge of an electron; K is the Boltzmann constant. Five unknown parameters I_L, I_o, R_s, R_{sh}, and A are, respectively, the light current, diode reverse saturation current, series resistance, shunt resistance, and the ideality factor of the diode.

At least five different boundary conditions are needed to calculate the value of these five parameters under the standard state. At short circuit, two boundary conditions can be obtained, they are (1): $V = 0$, $I = I_{sc,ref}$; (2) $[dI/dV]_{sc} = -1/R_{sh,ref}$; When the open voltage circuit is (3): $I = 0$, $V = V_{oc,ref}$; At maximum power point, there are also two boundary conditions, which are (4): $I = I_{mp,ref}$, $V = V_{mp,ref}$; (5) $[dVI/dV]_{mp} = 0$. By Substituting the above-mentioned boundary conditions into Eq. (39), the following equations can be obtained [11]:

Table 1
Relative parameters for the thermal model.

Parameter	Symbol	Value
coefficient of angularity	F_{pv-Fl}	0.194
coefficient of angularity	F_{pv-f}	0.806
Diffusion thermal resistance (K/W)	R_{ce1}	0.05
Diffusion thermal resistance (K/W)	R_{ce2}	0.017
equivalent thermal resistance (K/W)	R_{pv}	0.2
Contact thermal resistance between absorber plate and heat pipe (K/W)	R_{ct1}	0.0002
Contact thermal resistance between the condensing section of heat pipe and tube (K/W)	R_{ct2}	0.0001

$$I_{sc,ref} = I_{L,ref} - I_{o,ref}\left\{\exp\left[\frac{m\left(I_{sc,ref}R_{s,ref}\right)}{T_{ref}}\right] - 1\right\} - \frac{I_{sc,ref}R_{s,ref}}{R_{sh,ref}} \tag{40}$$

$$\frac{-\frac{mI_{o,ref}}{T_{ref}}\exp\left[\frac{m\left(I_{sc,ref}R_{s,ref}\right)}{T_{ref}}\right] - \frac{1}{R_{sh,ref}}}{1 + \frac{mI_{o,ref}R_{s,ref}}{T_{ref}}\exp\left[\frac{m\left(I_{sc,ref}R_{s,ref}\right)}{T_{ref}}\right] + \frac{R_{s,ref}}{R_{sh,ref}}} = -\frac{1}{R_{sh,ref}} \tag{41}$$

$$0 = I_{L,ref} - I_{o,ref}\left[\exp\left(\frac{mV_{oc,ref}}{T_{ref}}\right) - 1\right] - \frac{V_{oc,ref}}{R_{sh,ref}} \tag{42}$$

$$I_{mp,ref} = I_{L,ref} - I_{o,ref}\left\{\exp\left[\frac{m\left(V_{mp,ref} + I_{mp,ref}R_{s,ref}\right)}{T_{ref}}\right] - 1\right\} - \frac{V_{mp,ref} + I_{mp,ref}R_{s,ref}}{R_{sh,ref}} \tag{43}$$

$$\frac{-V_{mp,ref}\left\{\frac{mI_{o,ref}R_{s,ref}}{T_{ref}}\exp\left[\frac{m\left(V_{mp,ref}+I_{mp,ref}R_{s,ref}\right)}{T_{ref}}\right] + \frac{1}{R_{sh,ref}}\right\}}{1 + \frac{mI_{o,ref}R_{s,ref}}{T_{ref}}\exp\left[\frac{m\left(V_{mp,ref}+I_{mp,ref}R_{s,ref}\right)}{T_{ref}}\right] + \frac{R_{s,ref}}{R_{sh,ref}}} + I_{mp,ref} = 0 \tag{44}$$

where a parameter $m = q/(A \cdot k)$ is used in the equations to simplify the equations. The subscripts $_{mp}$, $_{sc}$, $_{oc}$ and $_{ref}$ correspond to the maximum power point, short circuit current, open circuit voltage, and reference point under standard state, respectively.

Sunlight is concentrated on the surface of PV cell, the I_L, I_o, and R_s vary with the temperature and the intensity of solar radiation according to the following equations [48]:

$$I_L = \frac{I_s}{I_{s,ref}}\left[CI_{L,ref} + \mu_{I_{sc}}\left(T_{pv} - T_{ref}\right)\right] \tag{45}$$

$$I_o = I_{o,ref}\left(\frac{T_{pv}}{T_{ref}}\right)^3 \exp\left(\frac{E_g}{KT_{ref}} - \frac{E_g}{KT_{pv}}\right) \tag{46}$$

$$R_s = R_{s,ref}\frac{T_{pv}}{T_{ref}}\left(1 + \beta ln\frac{I_s}{I_{s,ref}}\right) \tag{47}$$

where μ_{Isc} is the temperature coefficient of short circuit current; Eg is the bandgap energy; β is the radiation intensity coefficient of series resistance.

Assuming that R_{sh} and A have no dependence on the temperature of the PV cell, R_{sh} is not infinite and varies with intensity of solar radiation. They can be calculated by the following formula [48,49]:

$$A = A_{ref} \tag{48}$$

$$\frac{R_{sh}}{R_{sh,ref}} = \frac{I_{s,ref}}{I_s} \tag{49}$$

Then, the relationship between load voltage and output current can be obtained according to the equation above. The electrical output in equation (12) can be defined as:

$$E_p = V_{mp}I_{mp} \tag{50}$$

Table 2 shows the parameters for electrical model from the manufacturer.

2.4. Thermodynamic analysis

The electrical efficiency η_{el} is used to evaluate the CPV system, which is defined as the ratio of actual electrical output power to input solar radiation on the surface of Fresnel lens. And the quality of energy is considered in the exergy analysis [50,51],

$$\eta_{el} = \frac{E_p - P_{pump}}{A_{Fl}I_s} \tag{51}$$

The electrical exergy efficiency ξ_{el} of CPV system is defined as the ratio of work exergy rate to net input exergy rate. Work exergy rate includes the difference between output electrical power of PV and consumed electrical power by pump. The formulas of calculating η_{el} and ξ_{el} are as follows [52,53]:

$$\xi_{el} = \frac{E_p - P_{pump}}{A_{Fl}I_s\left[1 - \frac{4}{3}\left(\frac{T_a}{T_{sun}}\right) + \frac{1}{3}\left(\frac{T_a}{T_{sun}}\right)^4\right]} \tag{52}$$

where $P_{pump} = \Delta pQ_v$, represents the pump power consumption of the fan required for forced air cooling or the power consumption during flow pumping of the cooling fluid, which can be expressed by the following formulas:

$$P_{pump,air} = \frac{12\nu_{air}L_{cm}u_{air}}{\alpha_{air}}Q_{v,air} \tag{53}$$

$$P_{pump,w} = \frac{f\rho_w L_{cm}u_w^2}{2D_h}Q_{v,w} \tag{54}$$

In the previous equations, Δp, Q_v, ν_{air}, u_{air}, α_{air} and f are pressure drop of inlet and outlet air or water, volume flow of air or water, viscosity coefficient of air, forced wind velocity, thermal diffusivity of air and friction factor, respectively.

3. The experimental setup

In order to compare the performance of three different heat exchange modules under the same environmental conditions and their influence on the output power of the concentrating photovoltaic system, a preliminary small-scale experiment was carried out. The basic idea is to verify the mathematical model by testing the electrical characteristics of PV cells and testing the temperature of the experimental components of the CPV system such as absorber plate and cooling module. The CPV systems with different cooling devices are mounted on one tracking system, and the main test components are shown in Fig. 6. The experimental prototype

Table 2
The electrical parameters in the simulation model.

Parameter	Symbol	Value
Short circuit current under standard conditions	$I_{sc,ref}$	0.0141A/cm^2
Open circuit voltage under standard conditions	$V_{oc,ref}$	3.18 V
Current at the maximum power point under standard state	$I_{mp,ref}$	0.01364A/cm^2
Voltage at the maximum power point under standard state	$V_{mp,ref}$	2.8 V
Temperature coefficient of short circuit current	μ_{Isc}	0.00012 A/°C
Temperature coefficient of open circuit voltage	μ_{Voc}	-0.56 mV/°C

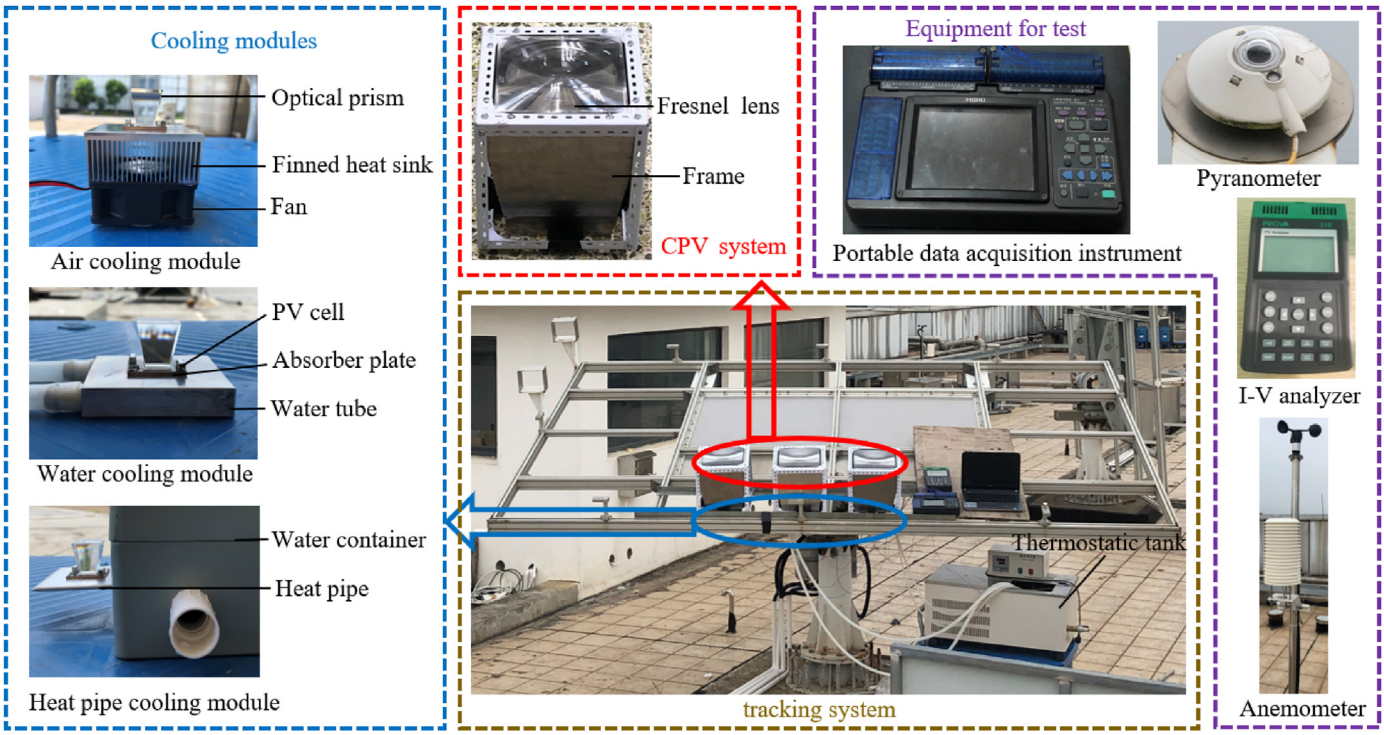

Fig. 6. The main experimental and test components.

consists of a Fresnel lens, a photovoltaic cell, a frame and three types of heat exchangers.

3.1. Experiment condition

The three identical PV cells used in experiments are the three-junction GaAs solar cells produced by SHENZHENYIXIN Photoelectric Equipment Ltd (product code: HGSC-A100B). The size of the PV cell is 10*10*1.2 mm. The open circuit voltage V_{oc} of the cell amounts to 3.18 V, and the short circuit current I_{sc} is 14.1 mA/cm^2. A solar module analyzer (PROVA210, 0-12A, 0-60 V) produced by TAIWANBAOHUA is implemented to measure the I-V curves of the PV cells. The measurement accuracies of current and voltage are both 1%. The temperatures of the CPV system components, ambient and cooling water are measured by using type-K thermocouples. The solar radiation obtained by a pyranometer, model CMP 10. The wind speed is measured with an anemometer, model DT3880. All sensors are connected to a portable data acquisition instrument, model LR8402-21 produced by HIOKI, which is used to record various measurement results. The CPV system is wrapped by an aluminum frame with the thickness of 2 mm. The upper and bottom sizes are 300*300 and 200*200 mm, which is used to reduce the heat input of the external environment to the photovoltaic cell, and also to support the entire assembly.

The prototype of three cooling modules are shown in Fig. 6. The dimension of the cross-sectional area of aluminum heatsink is 60*60 mm, and the thickness, height and pitch of the fins are 1, 36 and 2.1 mm respectively, while the base thickness is 3 mm. The wind velocity of the fan is controlled by a generator. Several temperature sensors are applied to measure the upper side temperatures of PV cells and absorber plate.

The length, width and height of the aluminum water-cooling module with an "M" shaped channel are 60 mm, 60 mm and 12 mm, while the thickness of the wall is about 1 mm, and the inner diameter of the channel is 10 mm. A hydraulic pump and a thermostatic tank (DC-1030) are used to drive the water flow and provide an adjustable cooling water temperature and velocity. Similar to the finned heatsink above, the thermocouples are connected to the edge of the PV cell, the surface of the absorber plate, and is also arranged at the inlet and outlet of the water-cooling module to monitor the water temperature. In addition, this module recognizes the pressure drop in the channel by measuring the inlet and outlet pressures.

The heat pipe module is mainly composed of a flat heat pipe, and a small water tank for cooling water. The equivalent diameter and length of the heat pipe are 5.6 mm and 160 mm respectively. The inner and outer equivalent diameters of the heat pipe wick with a micro groove structure are 3.47 mm and 3.87 mm. The working fluid inside the heat pipe is water. The PV cell is fixed on the upper surface of the heat pipe. This part is regarded as the evaporation section of the heat pipe, and its cross-sectional dimension is 60*60 mm. The remaining part is the condensation end, which is connected to the small water tank. Similarly, the thermocouples are additionally arranged on the surface of the evaporation and condensation section of the heat pipe.

The values of climatic, operating and detailed design parameters during validation process are provided in the following Table 3.

3.2. Experimental verification

Three CPV systems with different cooling methods were tested at a concentration ratio of 314 under steady-state and transient conditions on the same day of 11:30 to 12:30. The dynamic temperature of different cooling modules' top surface and the power output of the PV cells are obtained under the same solar radiation and environmental conditions. In order to verify the accuracy of the simulation models, the present mathematical models are calculated according to the relevant parameters of the experimental prototype, and the comparison between experimental results and simulation has been performed. The root-mean-square deviation

Table 3
Relative parameters in the experiment.

Component	Parameter	Symbol	Value
Fresnel lens	Transmittance	τ_{Fl}	0.92
	Absorptance	α_{Fl}	0.05
	Area (cm^2)	A_{Fl}	314
PV cell	Absorptance	α_{pv}	0.9
	Emittance	ε_{pv}	0.9
	Area (cm^2)	A_{pv}	1
	equivalent thermal resistance (K/W)	R_{pv}	0.2
	Diffusion thermal resistance (K/W)	R_{ce1}	0.05
Absorber plate	Area of absorber plate (cm^2)	A_{ap}	6
	Thickness (cm)	δ_{ap}	0.15
	Thermal conductivity ($W\cdot m^{-1}\cdot K^{-1}$)	k_{ap}	398
	Diffusion thermal resistance (K/W)	R_{ce2}	0.02
Frame	Area (cm^2)	A_f	34.25
Air-cooling module	Height (cm)	H_1	2.3
	Cross-sectional area (cm^2)	S_{cm1}	36
	Contact area with cooling fluid (cm^2)	A_{cm1}	956
	Length (cm)	L_{cm1}	6
	Flow rate of air (m/s)	μ_{air}	4
Water-cooling module	Height (cm)	H_2	1.2
	Cross-sectional area (cm^2)	S_{cm2}	36
	Contact area with cooling fluid (cm^2)	A_{cm2}	88
	Hydraulic diameter (cm)	D_h	1
	Flow rate of water (m/s)	μ_w	0.02
	Inlet temperature (K)	T_{in}	293
Heat pipe module	Cross-sectional area of the evaporation	S_{cm3}	36
	Contact area with cooling fluid (cm^2)	A_{cm3}	153
	Outer diameter of pipe (cm)	D_{op}	0.56
	Inner diameter of pipe (cm)	D_{ip}	0.387
	Outer diameter of core (cm)	D_{oc}	0.387
	Inner diameter of core (cm)	D_{ic}	0.347
	Length of the evaporation section (cm)	L_{ep}	6
	Length of the condensation section (cm)	L_{cp}	10
	Contact area with cooling fluid (cm^2)	A_{cm3}	125
	Flow rate of water (m/s)	μ_w	0.02

(RMSD) [54] is used to evaluate the fitness between them.

$$RMSD = \sqrt{\frac{\sum \left[\left(X_{\sin,i} - X_{\exp,i}\right)/X_{\exp,i}\right]^2}{n}} \tag{55}$$

where $X_{\sin,i}$ and $X_{\exp,i}$ are the simulated and experimental values, respectively. n refers to the number of experimental data.

The top surface temperature variations of the cooling modules measured in the experiment and calculated in the simulation with time under different environmental conditions are shown in Fig. 7. It can be seen that the experimental and simulated temperature results of the three cooling modules are well matched. The maximum temperature difference value between the simulation and experiment is within 2 °C, and the maximum error is no more than 5%. Specifically, the RMSD of the temperature of the air-cooling module, water-cooling module, and heat pipe cooling module is only 1.42%, 1.44%, and 1.53%, respectively. Therefore, those results indicate that the present models have a high accuracy to be used to simulate energy transfer in the CPV systems.

The data at 12:00 was selected to further compare the electrical performance. Fig. 8 shows the comparison of I-V curves and electrical output power curves between experiment and simulation. One can be found that the simulated results coincide well with the experimental data. The maximum error of electrical efficiency between experiment and simulation is less than 3%. The comparison between the experimental results and that of the simulation permits to validate the accuracy of models, which indicate the models can be used for further analysis to optimize the experiment.

4. Results and discussion

In this section, the cooling performance of different cooling modules and the I–V characteristic of the CPV system were comparatively investigated. The effects of concentration ratio, inlet fluid temperature and mass flow rate on output performance of the CPV system were studied by simulation. The experimental data at 12:00 was selected as the input parameter of the numerical models. When one parameter was studied, the others were kept unchanged.

4.1. Basic thermoelectric performance comparison

From the experimental and simulation results of Fig. 7 shows that the finned heat sink has relatively poor cooling performance, and the average temperature of the finned heat sink during the test is 41 °C. While the average temperature of water exchanger is 25.9 °C. The heat pipe cooling method could provide a better cooling effect than the water-cooling method, which keeps the temperature of the heat pipe at the lowest level of 22.2 °C. It can be seen from the peak value of the electrical power curves in Fig. 9 that the output power produced by PV cells is positively correlated with the heat exchange performance of cooling method used. The electrical output of PV cell increases with the improvement of cooling module performance. The CPV system with heat pipe cooling has the highest power output of 8.27 W, followed by the CPV system with water cooling, which has a power output of 8.17 W, while the output power of the CPV system with air cooling is 7.84 W.

The reason for this phenomenon could be explained as maintaining a lower temperature of the PV cell can make it have a higher

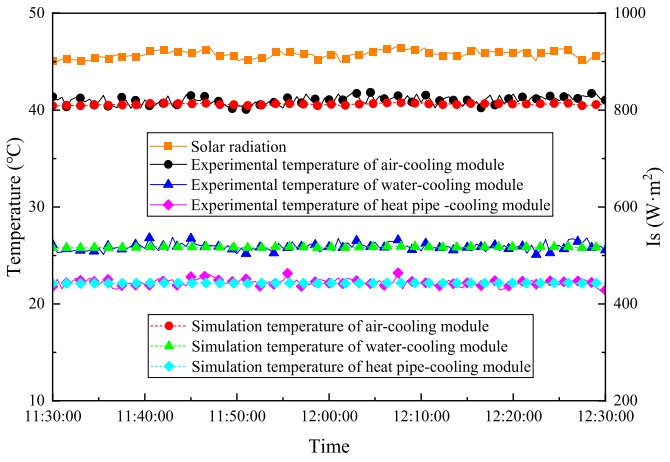

Fig. 7. Comparisons between the simulated temperature data and the results of experimental.

photoelectric conversion efficiency, and then a higher power output. The heat transfer capacity of water-cooling method is better than the air cooling because of its higher average heat transfer coefficient. While the thermal contact area between the heat pipe exchanger and cooling medium is nearly 1.8 times that of the water-cooling exchanger in our experiments. Therefore, the cooling effect of the heat pipe radiator is more obvious than that of the water-cooling radiator.

4.2. Net thermoelectric performance comparison

Fig. 9 (a) shows the measured results of the output power of PV cells and the power consumption of auxiliary devices of the three heat exchangers at 12:00 under the experimental conditions mentioned above in Table 3. The heat pipe cooling method shows a better heat transfer performance without considering the pump power loss because of the more effective area and mass flow rate. As shown in Fig. 9 (b), the CPV cell with heat pipe cooling technology has the highest electrical efficiency of 28.7%. The η_{el} of water-cooling method and air-cooling method is 28.4% and 27.2% respectively. However, the situation becomes different when considering the pump consumption. The water exchanger shows an effective and low-consumption method at operation condition. The electric efficiency with pump consumption and the electric exergy efficiency of the CPV cell cooled by water cooling method is 28.3% and 30.4%. The η_{el-net} and ξ_{el} of air-cooling method are 26.7% and 28.7%, and that of heat pipe cooling method are 28% and 30.1%. This is because both the air-cooling module and the heat pipe cooling module require more additional work to maintain a high mass flow rate under our experimental conditions, subsequently they present higher auxiliary consumption and lower net electrical efficiency than that of water cooling.

4.3. Different concentration ratio

From Fig. 10, it can be seen that the change electrical output power of three CPV system with different cooling methods is in an upward trend, but the increasing trend decreases slowly as the concentration ratio increases. As the concentration ratio rises from 100 to 1000, the output power produced by PV cells with air cooling, water cooling and heat pipe cooling method increases from 2.52 W to 23.43 W, from 2.61 W to 24.94 W and from 2.64 W to 25.53 W, respectively.

Fig. 11 shows the effect of concentration ratio on electrical efficiency of CPV system with different cooling method, from which one can observe that as the concentration ratio increases, the η_{el} of air-cooling, water-cooling and heat pipe cooling method changes from 27.5% to 25.6%, from 28.5% to 27.2% and from 28.7% to 27.8%. It can be noticed that the electrical efficiency does not change significantly from 100 to 600 concentration ratio, while the electrical efficiency shows a downward trend as the concentration ratio continues to increase. However, when considering pump consumption factors, both the net electrical efficiency and electrical exergy efficiency of the CPV system with three cooling modules show a trend of increases first and then decreases. Compared with the other selected concentration ratios, CPV cells with three cooling methods all exhibited higher net electrical efficiency and exergy efficiency at the concentrating ratios of 400-600. The CPV system with heat pipe cooling module shows the highest net electrical efficiency of 28.6% and electrical exergy of 30.8%. The maximum value of the η_{el-net} and ξ_{el} for the air-cooling module is 26.9% and 29%, and that for the water-cooling module is 28.5% and 30.6%.

This is because as the concentration ratio increases in the low and medium range, the initial total energy received by the PV cells also increases. At this time, the cooling method is sufficient to meet the cooling demand of the PV cells, and they are in the best working state, showing a relatively high photoelectric conversion efficiency, which is sufficient to cover the adverse effects of the rise in the temperature of the PV cell itself. It is worth noting that under a small concentration ratio, the excessive mass flow into the cooling

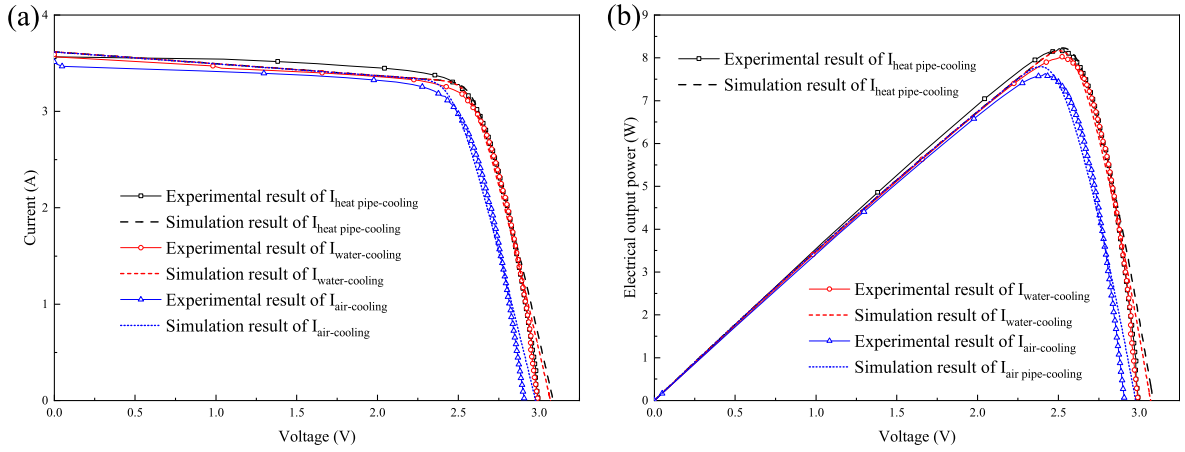

Fig. 8. Simulated and experimental results of CPV systems with different cooling module. (a) I–V curves. (b) Electrical output power curves.

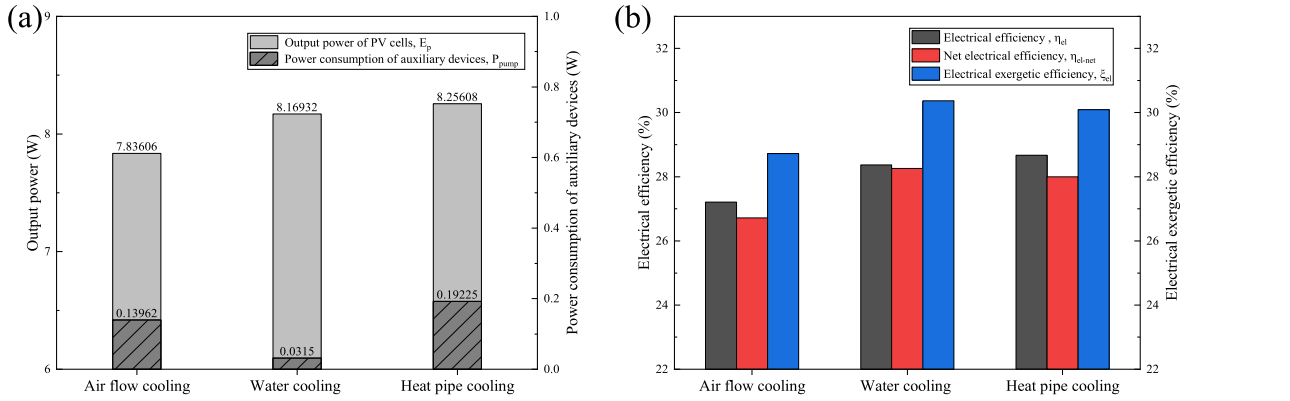

Fig. 9. (a) Output power and power consumption of PV cell with different cooling methods. (b) Electrical efficiency and electric exergy efficiency of PV cell with different cooling methods.

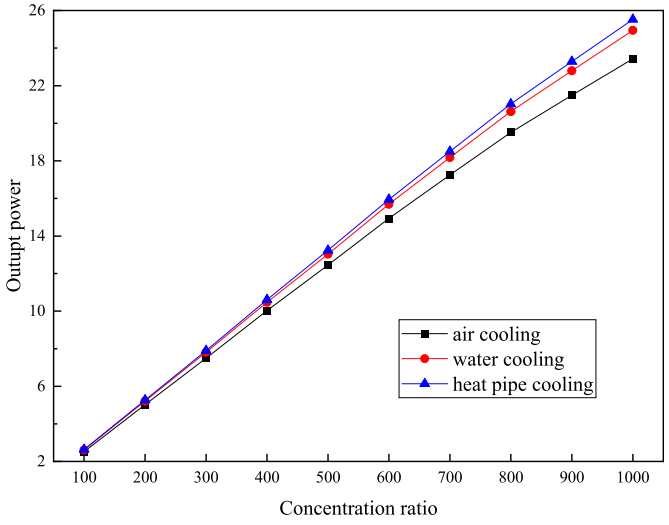

Fig. 10. Effect of concentration ratio on output power of PV cell with different cooling method.

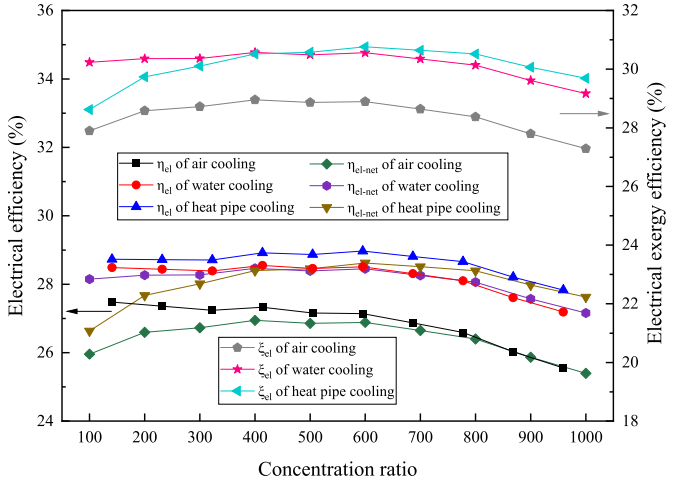

Fig. 11. Effect of concentration ratio on electrical efficiency of CPV system with different cooling method.

module will consume power in vain and reduce the electrical efficiency of the system. As the concentration ratio continues to increase from the middle range to the high range, the PV cell temperature rises more obviously, and the adverse effects brought by this are particularly obvious, which causes the electrical efficiency to continue to decrease. Considering the pump consumption, because the output power of the photovoltaic cell at a low concentration ratio is small, the electric efficiency and electric energy efficiency calculated by using Equation (52) and Equation (53) show smaller values. In addition, the PV cell with heat pipe cooling module shows the highest output power at all concentration ratios. This is because the heat transfer performance of the heat pipe is better under each selected working condition.

4.4. Comparisons under different temperature of cooling fluid

The effect of inlet temperature of fluid on output power of the CPV system is shown in Fig. 12. As the inlet temperature of cooling fluid increases from 0 °C to 50 °C, the output power produced by PV cells with air cooling, water cooling and heat pipe cooling method decreases by 7.4% from 8.2 W to 7.59 W, by 6.9% from 8.4 W to 7.82 W and by 7.3% from 8.51 W to 7.89 W, respectively. Among the three cooling methods, the CPV system using the air-cooling

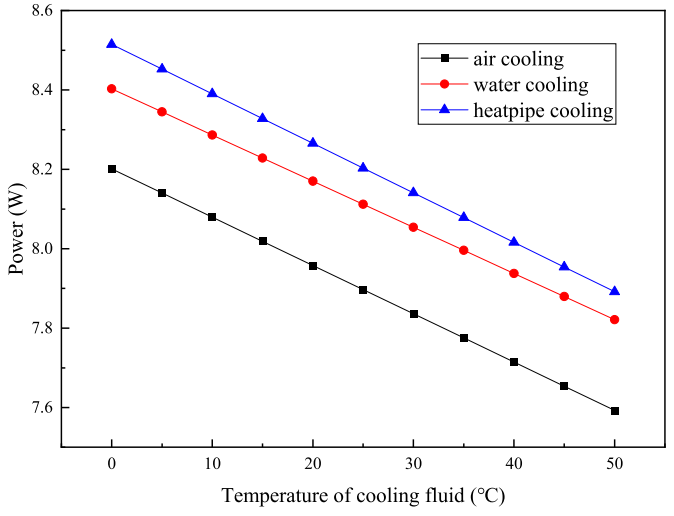

Fig. 12. Effect of inlet temperature of fluid on output power of PV cell with different cooling method.

module is more sensitive to the inlet temperature due to the poor cooling performance. As shown in Fig. 13, the η_{el}, η_{el-net} and ξ_{el} are

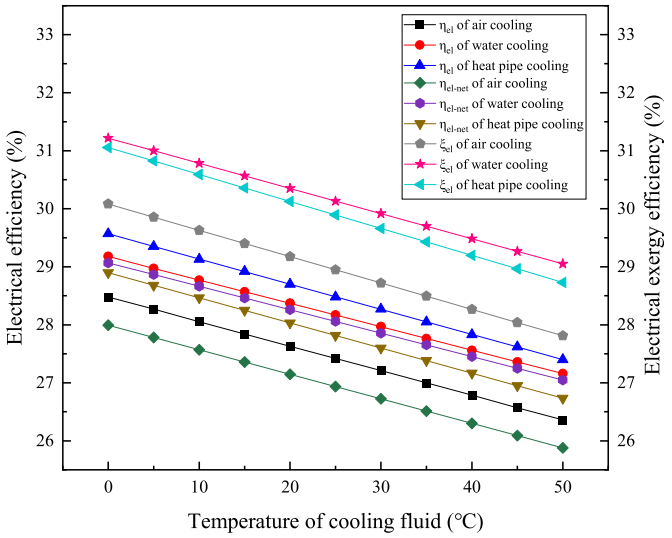

Fig. 13. Effect of inlet temperature of fluid on electrical efficiency of CPV system with different cooling method.

and 31.2%. The η_{el-net} and ξ_{el} of heat pipe cooling method are 28.9% and 31.1%, and that of air-cooling method are 28% and 30.1%. These results indicated that the inlet temperature of cooling fluid has a negative influence on the electrical output performance of the CPV cells.

4.5. Comparisons under different mass flow rates of cooling fluid

From Fig. 14 and Fig. 15, it can be seen that with the increase of the mass flow rate, the output power of three cooling methods show a trend of increasing first and then leveling off, and the power consumption of auxiliary device all increasing gradually. When the mass flow rate of cooling medium is 0.016, 0.001 and 0.003 kg/s, the output power of air-cooling, water-cooling and heat pipe cooling method is 7.87, 8.17 and 8.27 W, respectively. The corresponding η_{el} is 27.3%, 28.4% and 28.7%. It is worth noting that when the mass flow rate is greater than the above values, the changes in output power and η_{el} are less obvious. As shown in Fig. 15, with the increase of the mass flow rate, the η_{el} of three cooling methods first increase and then tend to be stable, while both the η_{el-net} and ξ_{el} increase first and then decrease. For air-cooling module, when the

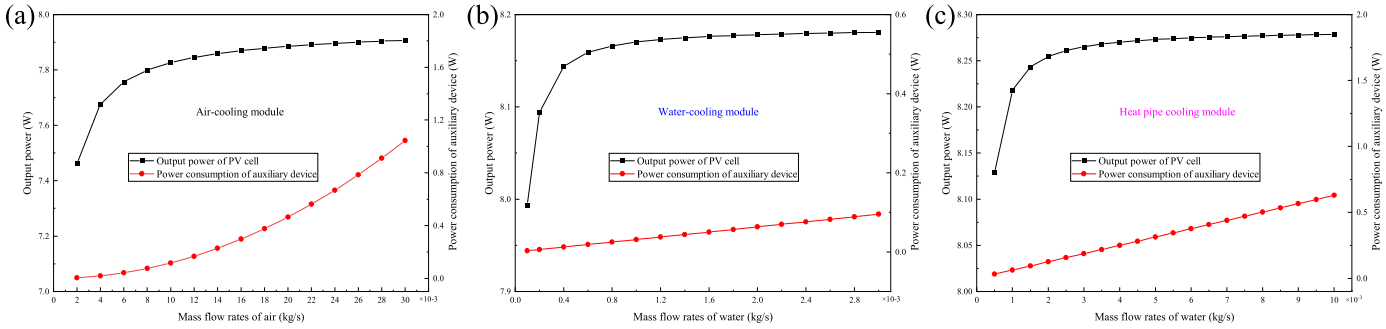

Fig. 14. Effect of mass flow rates of cooling medium on output power of PV cell with different cooling methods. (a) Air-cooling module. (b) Water-cooling module. (c) Heat pipe cooling module.

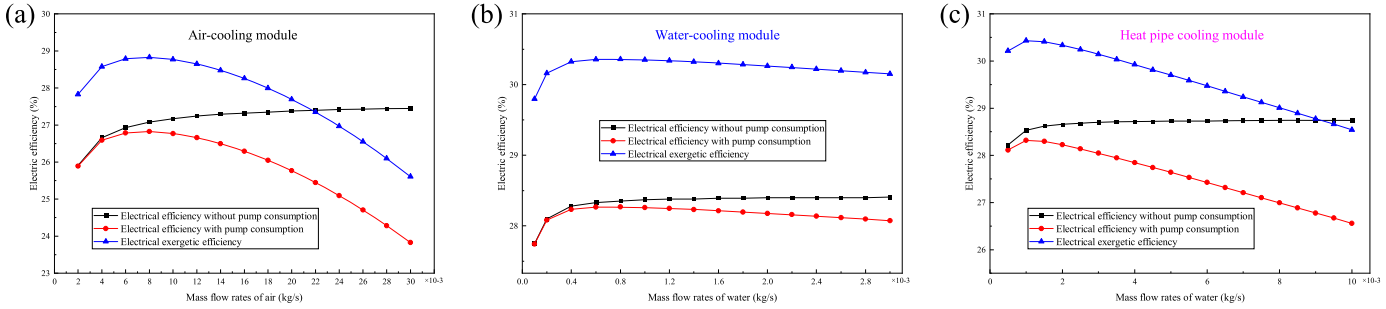

Fig. 15. Effect of mass flow rates of cooling medium on electrical efficiency of PV cell with different cooling methods. (a) Air-cooling module. (b) Water-cooling module. (c) Heat pipe cooling module.

all counter proportionable inlet temperature of cooling fluid, so they show a downward trend. At all inlet temperatures of the cooling fluid, the heat pipe cooling method exhibits the highest cooling performance, followed by water-cooling module and air-cooling module. When the inlet temperature of cooling medium is set to be 0 °C, the η_{el} of the PV cell with the heat pipe cooling, water-cooling and air-cooling module is 29.6%, 29.2% and 28.5%, respectively. However, due to the high pump loss of the air-cooling module and the heat pipe cooling module, CPV system with water-cooling module can produce the maximum η_{el-net} and ξ_{el} of 29.1% mass flow is 0.008 kg/s, the maximum values of η_{el-net} and ξ_{el} are 26.8% and 28.8%, respectively. For water-cooling module and when the mass flow is 0.0008 kg/s, the maximum values of η_{el-net} and ξ_{el} are 28.3% and 30.4%, respectively. It can also be observed that the maximum values of η_{el-net} and ξ_{el} for water cooling are 28.3% and 30.4%, which are very close to the values for heat pipe cooling, and their corresponding mass flow rates are 0.0008 kg/s and 0.001 kg/s, respectively.

5. Conclusion

In this work, this paper focuses mainly on three typical cooling methods commonly used in CPV systems: air cooling, water cooling and heat pipe cooling. Experimental and simulation methods were developed to investigate the cooling performance and electrical performance of the system. The main conclusions are summarized as follows:

(1) Through experiment, the cooling performance of the heat pipe cooling method is the best, the average temperature of the module is 22.2 °C, followed by the water-cooling module with an average temperature of 25.9 °C, and then the air-cooling module with an average temperature of 41 °C. The results show that the heat exchangers can be made more efficient by increasing the heat transfer coefficient and improving the scalability of the thermal contact area.
(2) The experimental results also show that when the pump power loss is not considered, the CPV system with heat pipe cooling provides the highest output power and electrical efficiency, which are 8.26 W and 28.7%, respectively. When the pump consumption factor is taken into account, the CPV system with the water-cooling module exhibits the highest net electrical efficiency and exergy efficiency of 28.3% and 30.4%, respectively, due to the least additional work required to maintain the mass flow.
(3) The established thermal models and electrical models are analyzed in detail. The comparison between the experimental results and that of the simulation permit to validate the accuracy of model. It indicates that the models can be further generalized to the analysis and optimization of PV farms.
(4) The simulation results show that the increase of the concentration ratio has a negative impact on the electrical efficiency of the CPV system. The electrical efficiency of CPV system can be improved by reducing the temperature of cooling medium as much as possible. The recommended flow rates for air cooling, water cooling and heat pipe cooling are respectively 0.004–0.01 kg/s, 0.0004–0.001 kg/s and 0.001–0.002 kg/s, which can provide considerable output under low pump consumption conditions.

Credit author statement

Ji Yishuang: Conceptualization, Methodology, Software, Writing – original draft, Writing – review & editing, Visualization. Lv Song: Conceptualization, Writing- Reviewing and Editing, Supervision. Qian Zuoqin: Resources, Conceptualization. Ji Yitong: Conceptualization, Methodology, Validation, Investigation, Supervision. Ren Juwen: Investigation, Methodology, Data curation. Kaiming Liang: Investigation, Methodology, Software. Shulong Wang: Investigation, Writing- Reviewing and Editing.

Declaration of competing interest

The authors declare that they have no known competing financial interests or personal relationships that could have appeared to influence the work reported in this paper.

Acknowledgments

This study was sponsored by the National Natural Science Foundation of China (NSFC 52106268).

References

[1] Kasaeian A, et al. Solar-driven polygeneration systems: recent progress and outlook. Appl Energy 2020:264.
[2] Gharzi M, et al. Progressive cooling technologies of photovoltaic and concentrated photovoltaic modules: a review of fundamentals, thermal aspects, nanotechnology utilization and enhancing performance. Sol Energy 2020;211:117–46.
[3] Hasan A, Sarwar J, Shah AH. Concentrated photovoltaic: a review of thermal aspects, challenges and opportunities. Renew Sustain Energy Rev 2018;94:835–52.
[4] Do KH, et al. General correlation of a natural convective heat sink with plate-fins for high concentrating photovoltaic module cooling. Sol Energy 2012;86(9):2725–34.
[5] Sangani CS, Solanki CS. Experimental evaluation of V-trough (2 suns) PV concentrator system using commercial PV modules. Sol Energy Mater Sol Cell 2007;91(6):453–9.
[6] Wang YN, et al. Numerical investigation of high-concentration photovoltaic module heat dissipation. Renew Energy 2013;50:20–6.
[7] Amanlou Y, et al. Air cooling low concentrated photovoltaic/thermal (LCPV/T) solar collector to approach uniform temperature distribution on the PV plate. Appl Therm Eng 2018;141:413–21.
[8] Al-Amri F, Mallick TK. Alleviating operating temperature of concentration solar cell by air active cooling and surface radiation. Appl Therm Eng 2013;59(1–2):348–54.
[9] Do KH, et al. General correlation of a natural convective heat sink with plate-fins for high concentrating photovoltaic module cooling (vol 86, pg 2725, 2012) Sol Energy 2013;94. 367–367.
[10] Kumar NS, et al. Experimental validation of a heat transfer model for concentrating photovoltaic system. Appl Therm Eng 2012;33–34:175–82.
[11] Yousef MS, Rahman AKA, Ookawara S. Performance investigation of low - concentration photovoltaic systems under hot and arid conditions: experimental and numerical results. Energy Convers Manag 2016;128:82–94.
[12] Renno C, Petito F. Design and modeling of a concentrating photovoltaic thermal (CPV/T) system for a domestic application. Energy Build 2013;62:392–402.
[13] Tan WC, Chong KK, Tan MH. Performance study of water-cooled multiple-channel heat sinks in the application of ultra-high concentrator photovoltaic system. Sol Energy 2017;147:314–27.
[14] Chemisana D, Ibanez M, Rosell JI. Characterization of a photovoltaic-thermal module for Fresnel linear concentrator. Energy Convers Manag 2011;52(10):3234–40.
[15] Du B, Hu E, Kolhe M. Performance analysis of water cooled concentrated photovoltaic (CPV) system. Renew Sustain Energy Rev 2012;16(9):6732–6.
[16] Liang K, et al. The comparison study between different battery and channel of the LCPV/T systems under concentration ratio 4. Energy 2020:191.
[17] Soliman AMA, Hassan H. An experimental work on the performance of solar cell cooled by flat heat pipe. J Therm Anal Calorim 2021;146(4):1883–92.
[18] Esen M, Esen H. Experimental investigation of a two-phase closed thermosyphon solar water heater. Sol Energy 2005;79(5):459–68.
[19] Han XY, Zhao XB, Chen XB. Design and analysis of a concentrating PV/T system with nano fl uid based spectral beam splitter and heat pipe cooling. Renew Energy 2020;162:55–70.
[20] Chen HP, et al. Experimental investigation of a novel LCPV/T system with micro-channel heat pipe array. Renew Energy 2018;115:773–82.
[21] Esen M. Thermal performance of a solar cooker integrated vacuum-tube collector with heat pipes containing different refrigerants. Sol Energy 2004;76(6):751–7.
[22] Da Y, Xuan YM, Li Q. From light trapping to solar energy utilization: a novel photovoltaic-thermoelectric hybrid system to fully utilize solar spectrum. Energy 2016;95:200–10.
[23] Lamba R, Kaushik SC. Modeling and performance analysis of a concentrated photovoltaic-thermoelectric hybrid power generation system. Energy Convers Manag 2016;115:288–98.
[24] Najafi H, Woodbury KA. Optimization of a cooling system based on Peltier effect for photovoltaic cells. Sol Energy 2013;91:152–60.
[25] Emam M, Radwan A, Ahmed M. Analysis of a new hybrid water-phase change material heat sink for low concentrated photovoltaic systems. Proc Asme Int Mech Eng Congr Expos 2018;6. 2017.
[26] Manikandan S, et al. Thermal management of low concentrated photovoltaic module with phase change material. J Clean Prod 2019;219:359–67.
[27] Emam M, Ahmed M, Ookawara S. Cooling of concentrated photovoltaic system using various configurations of phase-change material heat sink. Proc Asme Int Mech Eng Congr Expos 2016;6a. 2017.
[28] Han XY, Wang YP, Zhu L. Electrical and thermal performance of silicon concentrator solar cells immersed in dielectric liquids. Appl Energy 2011;88(12):4481–9.
[29] Han XY, Wang YP, Zhu L. The performance and long-term stability of silicon concentrator solar cells immersed in dielectric liquids. Energy Convers Manag 2013;66:189–98.
[30] An W, et al. Experimental investigation of a concentrating PV/T collector with Cu9S5 nanofluid spectral splitting filter. Appl Energy 2016;184:197–206.
[31] Wang G, et al. Thermodynamic and optical analyses of a hybrid solar CPV/T system with high solar concentrating uniformity based on spectral beam

splitting technology. Energy 2019;166:256–66.
[32] Liu Y, et al. Thermodynamic and optical analysis for a CPV/T hybrid system with beam splitter and fully tracked linear Fresnel reflector concentrator utilizing sloped panels. Sol Energy 2014;103:191–9.
[33] Radwan A, Ahmed M. The influence of microchannel heat sink configurations on the performance of low concentrator photovoltaic systems. Appl Energy 2017;206:594–611.
[34] Yang KJ, Zuo CC. A novel multi-layer manifold microchannel cooling system for concentrating photovoltaic cells. Energy Convers Manag 2015;89:214–21.
[35] Aldossary A, Mahmoud S, Al-Dadah R. Technical feasibility study of passive and active cooling for concentrator PV in harsh environment. Appl Therm Eng 2016;100:490–500.
[36] Chen HF, et al. Experimental and numerical comparative investigation on a concentrating photovoltaic system. J Clean Prod 2018;174:1288–98.
[37] Anderson WG, et al. In: Heat pipe cooling of concentrating photovoltaic cells. Pvsc: 2008 33rd Ieee photovoltaic specialists conference, vols. 1–4; 2008. p. 905–10.
[38] Farahat MA. In: Improvement the thermal electric performance of a photovoltaic cells by cooling and concentration techniques, in *IEEE 39th international universities power engineering conference*; 2004. p. 623–8.
[39] Lee DI, Baek SW. Development of a heating system using CPV technology and heat pipes. Environ Prog Sustain Energy 2015;34(4):1197–207.
[40] Yazdanifard F, Ebrahimnia-Bajestan E, Ameri M. Investigating the performance of a water-based photovoltaic/thermal (PV/T) collector in laminar and turbulent flow regime. Renew Energy 2016;99:295–306.
[41] Elsherbiny SM, Ismail OI. Heat transfer in inclined air rectangular cavities with two localized heat sources. Alex Eng J 2015;54(4):917–27.
[42] Lv S, et al. Design, fabrication and feasibility analysis of a thermo-electric wearable helmet. Appl Therm Eng 2016;109:138–46.
[43] Cui TF, Xuan YM, Li Q. Design of a novel concentrating photovoltaic-thermoelectric system incorporated with phase change materials. Energy Convers Manag 2016;112:49–60.
[44] Araiz M, et al. Experimental and computational study on thermoelectric generators using thermosyphons with phase change as heat exchangers. Energy Convers Manag 2017;137:155–64.
[45] Li GQ, et al. Performance analysis on a solar concentrating thermoelectric generator using the micro-channel heat pipe array. Energy Convers Manag 2016;112:191–8.
[46] Pei G, et al. Annual analysis of heat pipe PV/T systems for domestic hot water and electricity production. Energy Convers Manag 2012;56:8–21.
[47] De Soto W, Klein SA, Beckman WA. Improvement and validation of a model for photovoltaic array performance. Sol Energy 2006;80(1):78–88.
[48] Bahaidarah HM, et al. Experimental and numerical study on non-concentrating and symmetric unglazed compound parabolic photovoltaic concentration systems. Appl Energy 2014;136:527–36.
[49] Sarhaddi F, et al. An improved thermal and electrical model for a solar photovoltaic thermal (PV/T) air collector. Appl Energy 2010;87(7):2328–39.
[50] Akyuz E, et al. A novel approach for estimation of photovoltaic exergy efficiency. Energy 2012;44(1):1059–66.
[51] Esen H, et al. Energy and exergy analysis of a ground-coupled heat pump system with two horizontal ground heat exchangers. Build Environ 2007;42(10):3606–15.
[52] Sobhnamayan F, et al. Optimization of a solar photovoltaic thermal (PV/T) water collector based on exergy concept. Renew Energy 2014;68:356–65.
[53] Chen GL, et al. A visibly transparent radiative cooling film with self-cleaning function produced by solution processing. J Mater Sci Technol 2021;90:76–84.
[54] Bahaidarah H, et al. Performance evaluation of a PV (photovoltaic) module by back surface water cooling for hot climatic conditions. Energy 2013;59:445–53.